

Effect of Y_2O_3 -addition on the crystallographic and mechanical properties of the Ce-TZP/ Al_2O_3 composite

C. C. Gall¹, M. F. R. P. Alves², T. M. B. Campos³, C. dos Santos^{4,5}, P. L. Gomes^{4*}, G. R. Barbosa¹, E. S. Lima¹

¹Instituto Militar de Engenharia, 22290-270, Rio de Janeiro, RJ, Brazil

²Universidade de Aveiro, 3810-193, Aveiro, Portugal

³Universidade de São Paulo, Faculdade de Odontologia de Bauru, Departamento de Prótese e Periodontia, 17012-230, Bauru, SP, Brazil

⁴Universidade Federal Fluminense, Escola de Engenharia Industrial Metalúrgica de Volta Redonda, 27276-210, Volta Redonda, RJ, Brazil

⁵Universidade do Estado do Rio de Janeiro, Faculdade de Tecnologia, 27537-000, Resende, RJ, Brazil

Abstract

The effect of adding different Y_2O_3 contents on the physical and mechanical properties of Ce-TZP/ Al_2O_3 composites was investigated. Ce-TZP/ Al_2O_3 powder blends containing 1~10 wt% Y_2O_3 were compacted at 100 MPa-30 s and sintered at 1500 °C-2 h or 1600 °C-2 h. The materials were characterized by X-ray diffraction and scanning electron microscopy, Raman spectroscopy, relative density, and the mechanical properties of Vickers hardness and fracture toughness. After sintering, the relative density of the sintered samples varied between 92.7% and 96.3%. Furthermore, the addition of Y_2O_3 resulted in an increase in the amount of cubic zirconia (c- ZrO_2) and an increase in grain size in relation to the sample without the addition of Y_2O_3 . With the increase of Y_2O_3 in the composition and consequent increase in the cubic ZrO_2 phase content, although the hardness values did not present statistically significant variations, indicating average value of 12 GPa, a decrease in fracture toughness values was observed (10.0~5.5 MPa.m^{1/2}) as a direct function of the reduction in the population of tetragonal zirconia grains, responsible for the toughening mechanism by phase transformation in these composites.

Keywords: Ce-TZP/ Al_2O_3 , Y_2O_3 composite, Rietveld refinement, Raman spectroscopy, mechanical properties.

INTRODUCTION

For decades, ceramic materials have been widely used because of their high hardness, high compressive strength, and low density despite their brittle behavior [1]. Due to their mechanical properties, structural ceramics have shown increasing interest in different areas of application such as the automotive sector, and ballistic protection devices, in addition to the already known uses as abrasives and filters [2]. Furthermore, some ceramic materials, such as zirconia, are used in prostheses and hydroxyapatite as bone graft. Ceramic materials based on 3Y-TZP (polycrystalline tetragonal zirconia stabilized with 3 mol% Y_2O_3) are among the most promising materials used recently because, when well densified, they present high flexural strength, fracture toughness, and biocompatibility [3]. This condition makes Ce-TZP composites (ceria-stabilized polycrystalline tetragonal zirconia) an interesting alternative, as these materials have high toughness (9-14 MPa.m^{1/2}) and good flexural strength (500-700 MPa) [4-6]. The excellent performance of tetragonal-zirconia (t- ZrO_2) polymorph already investigated in medical and engineering applications, is mainly due to the toughening mechanism

of martensitic transformation from the tetragonal phase to the monoclinic phase (t→m), which hinders the growth of cracks with a consequent increase in the fracture toughness of the material [5]. On the other hand, in the presence of water or humid environments, surface t- ZrO_2 grains are subject to the phenomenon of aging, showing surface hydrothermal degradation, with the generation of microcracks, which cause loss of mechanical strength in the medium term [7].

In recent decades, zirconia matrix composites have been developed with the aim of increasing mechanical properties and resistance to hydrothermal degradation. An interesting class is nanocomposites rich in zirconia doped with oxides such as ceria, yttria, magnesia, and calcia for tetragonal phase stabilization [8]. Studies show that Ce-TZP/ Al_2O_3 composites have shown great potential as structural ceramics. Although the flexural strength is equal to that of conventional Y-TZP, the fracture toughness of Ce-TZP/ Al_2O_3 composites is significantly higher [9-12]. In view of their properties, it is important to develop new ways to provide cost reduction and make the material more efficient in the function it will perform. Another relevant field of application for zirconia-based ceramics focuses on electrical properties. In this context, cubic zirconia (c- ZrO_2) stands out. These materials have the characteristics of being fast oxide ionic conductors at high temperatures. Due to its high stability in reducing and oxidizing environments, c- ZrO_2 has

*patrickdelimavieira@hotmail.com

<https://orcid.org/0000-0002-5711-0943>

been used as an electrolyte material for solid oxide fuel cells and oxygen sensors. Despite these advantages, the room and high-temperature mechanical properties of cubic zirconia are quite low. Therefore, it is necessary to improve the mechanical properties of cubic zirconia to ensure the service life and reliability of the solid oxide fuel cell system [13].

Generally, the properties of ceramics depend on the microstructure. Many researchers have shown that the dispersion of nanoparticles in matrix grains is an effective technique to improve the mechanical properties of ceramics without deteriorating the electrical conductivity. Therefore, an experimental strategy would be the controlled addition of dopants to zirconia, such as Y_2O_3 , to form the cubic phase. In this sense, our work aims, on a preliminary basis, to investigate the physical and mechanical properties of a premixed commercial ceramic composite based on Ce-TZP/ Al_2O_3 doped with different Y_2O_3 contents.

EXPERIMENTAL

A nanoparticle ceramic powder of ceria-stabilized tetragonal zirconia with the addition of alumina (Ce-TZP/ Al_2O_3 , UprYZr-Shock, Saint Gobain) and a high purity yttrium oxide powder (Y_2O_3 , Alfa Aesar) were used. Material specifications are shown in Table I.

Mixtures of Ce-TZP/ Al_2O_3 powder containing 0, 1, 5, or 10 wt% Y_2O_3 were prepared by wet mixing adding isopropyl alcohol in a planetary ball mill (Pulverisette 5, Fritsch, Germany) at 400 rpm for 2 h. Then the mixtures were dried in an oven at 100 °C-24 h and sieved through a 250 μm sieve. To each powder mixture, deposited in a beaker, 4% polyethylene glycol binder (PEG 400, Synth) was added using a manual mixer (Haüskraft, China). After mixing, the powders were sieved again through a sieve of 32 μm . Samples (disc $\phi 20 \times 3$ mm), $n=5$ /group, were compacted by uniaxial pressing at 100 MPa-30 s. Sintering was carried out in a $MoSi_2$ resistance furnace (F-1700, Fortelab, Brazil). Temperatures of 1500 °C-2 h or 1600 °C-2 h were used. The heating and cooling rates used were 1 and 5 °C/min, respectively.

Table I - Characteristics of the raw materials used (manufacturer's data).

Characteristic	Ce-TZP/ Al_2O_3 ^a	Y_2O_3 ^b
ZrO ₂ (wt%)	Balance	-
CeO ₂ (wt%)	6±0.7	-
Al_2O_3 (wt%)	15±1	-
SiO ₂ +Na ₂ O (wt%)	<0.04	-
TiO ₂ (wt%)	<0.005	-
Y_2O_3 (wt%)	-	99.995
Density (g/cm ³)	5.65	5.01
Average particle size (μm)	0.25	0.2
Specific surface area (m ² /g)	8.5	*

^a: UprYZr-Shock (Saint-Gobain, France); ^bREO (Alfa Aesar, USA); * not evaluated.

The real specific mass of the Ce-TZP/ Al_2O_3 and nanometric Y_2O_3 powders was obtained by helium pycnometry (Ultracycrometer/1000, Quantachome). The apparent density of the sintered products was determined by applying the Archimedes principle using a precision scale and then, the values were correlated with the theoretical densities of the mixtures obtained by the rule of mixture. The crystalline phases of the powders and sintered samples were determined by X-ray diffraction (XRD) with a diffractometer (X'Pert-Pro, Panalytical). The analyses were carried out in the 2 θ scanning range between 20° and 80°, angular step of 0.03°, and collection time of 150 s, using cobalt radiation (1.789 Å), voltage of 40 kV, and current of 40 mA. The quantification of the crystalline phases was obtained by the Rietveld method. The sintered composites were also evaluated using confocal-type Raman spectroscopy equipment (LabRAM HR Evolution, Horiba). The spectra were recorded in the range between 0 and 800 cm⁻¹ with an acquisition time of 30 s. The sintered samples were sanded and then polished, using diamond pastes of 9, 6, 3, and 1 μm , for microstructural and mechanical characterizations. Microstructural analyses were performed with a scanning electron microscope (SEM, Quanta 250 FEG, FEI). For the microstructural characterization, the samples were thermally etched at 1400 °C-15 min in a furnace (FE-1750, Maitec, Brazil). After this procedure, the polished surface of the samples was covered with a thin layer of gold using a metallizer. The average grain size was measured through the images obtained, using the average Feret's diameter method through the automatic image analysis of the Image J software. Vickers hardness was measured following the recommendations of the ASTM C1327 standard [14], applying an indentation load of 10 kgf (98 N), with an application time of 15 s, using 10 indentations/sample using a microhardness tester (DuraScan 50 DS-50, Emcotest). Furthermore, fracture toughness was determined by the Vickers indentation fracture (IF) method, in which the cracks radiating from the indentation vertices were measured immediately after the hardness indentations, using the model proposed by Niihara [15] valid for Palmqvist-type cracks, which have a crack length (c) and indentation size (a) ratio, $c/a < 2.5$. Crystalline phases of the sintered samples were also evaluated using a confocal type Raman spectroscopy (LabRAM HR Evolution, Horiba). The spectra were recorded between 0 and 1000 cm⁻¹ with

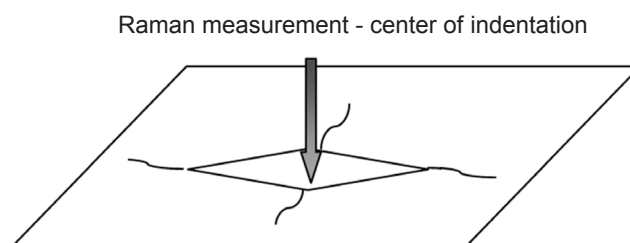


Figure 1: Schematic representation of the position of Raman measurements after indentation.

an acquisition time of 30 s, 2 cycles, and a slit size of 100 μm . Quantitative phase analysis was carried out using the model proposed by Clarke and Adar [16]. The identification of the phase transformation around the indentations was performed by measuring the center of the indentations as shown in Fig. 1.

RESULTS AND DISCUSSION

XRD patterns of the starting powders are shown in Fig. 2 and the results of the Rietveld refinement are presented in Table II. It was possible to identify in the commercial Ce-TZP/ Al_2O_3 powder the presence of ZrO_2 in the monoclinic, m- ZrO_2 (77.1%), and tetragonal, t- ZrO_2 (4.3%) phases, in addition to 14.2% hexagonal Al_2O_3 and 4.4% CeO_2 .

The relative density results referring to the sintered samples are shown in Fig. 3. It was observed that the composites showed relative density values ranging between 92.4 \pm 3.4% and 96.3 \pm 4.1%, for different compositions, with a slight tendency towards increased densification with the increase in the sintering temperature (1500 to 1600 $^\circ\text{C}$). Furthermore, there was no well-defined correlation between relative density and the yttria content added to the original mix of commercial powders. This behavior was related to phase transformations that occurred concurrently

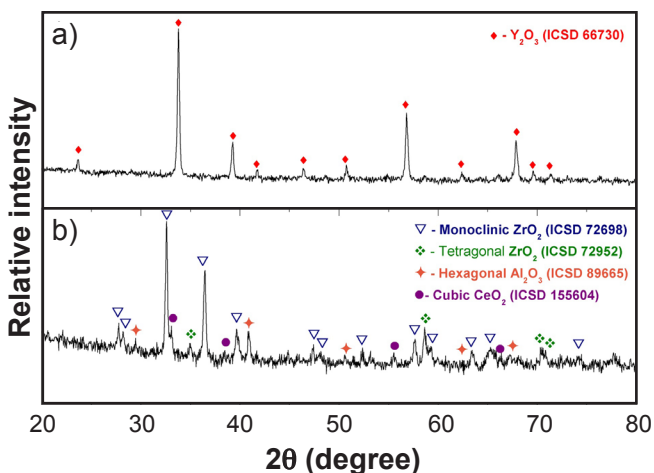


Figure 2: XRD patterns of the starting powders: a) Y_2O_3 ; and b) Ce-TZP/ Al_2O_3 .

with the densification of the composites, with emphasis on the incorporation of Y_2O_3 into zirconia grains that occurred during heating, as is discussed later. Inokoshi et al. [7] studied samples of commercial zirconia containing alumina with sintering temperatures of 1450, 1550, and 1650 $^\circ\text{C}$ and soaking times of 1, 2, and 4 h; they observed that the relative density decreased as a function of the sintering temperature. The authors used the phenomenon described by Lange [17] as a justification, where densification was related to grain growth or even to the increase in the cubic and monoclinic phase of lower density due to phase transformation. The densities found were similar to the results of the research by Naga et al. [18] who used an alumina/YAG/ CeO_2 composite, obtaining values between 86% and 98%. The results can also be compared to the other research by Naga et al. [19] where a composite of $\text{ZrO}_2/\text{Al}_2\text{O}_3$ doped with Y_2O_3 - CeO_2 was studied, with results that were between 2.8 and 5.0 g/cm^3 .

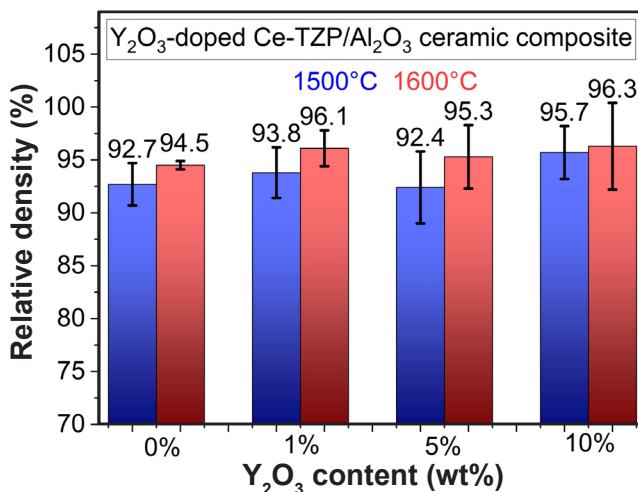


Figure 3: Relative density as a function of yttria content and sintering temperature.

Figs. 4a and 4b show the X-ray diffractograms of samples sintered at 1500 and 1600 $^\circ\text{C}$, respectively. In a qualitative analysis, it was possible to observe in the diffractograms that all compositions showed peaks of phases t- ZrO_2 , c- ZrO_2 , and Al_2O_3 . In addition to these phases, m- ZrO_2 was found in Ce-TZP/ Al_2O_3 samples and those that were doped with 1 wt% Y_2O_3 . A peak referring to the sample holder of the

Table II - Crystallographic characteristics of the Y_2O_3 and Ce-TZP/ Al_2O_3 composite from XRD analysis.

Parameter	Y_2O_3		Ce-TZP/ Al_2O_3		
	Y_2O_3	m- ZrO_2	t- ZrO_2	CeO_2	Al_2O_3
Crystalline phase	Y_2O_3	m- ZrO_2	t- ZrO_2	CeO_2	Al_2O_3
Content (%)	100	77.1	4.3	4.4	14.2
System	Cubic	Monoclinic	Tetragonal	Cubic	Hexagonal
Space group	Ia-3 (n° 206)				
a (Å)	10.6079(3)		Not evaluated		
$R_p/R_{wp}/R_{exp}$ (%)	9.2/15.4/11.3				
χ^2	1.88		1.78		

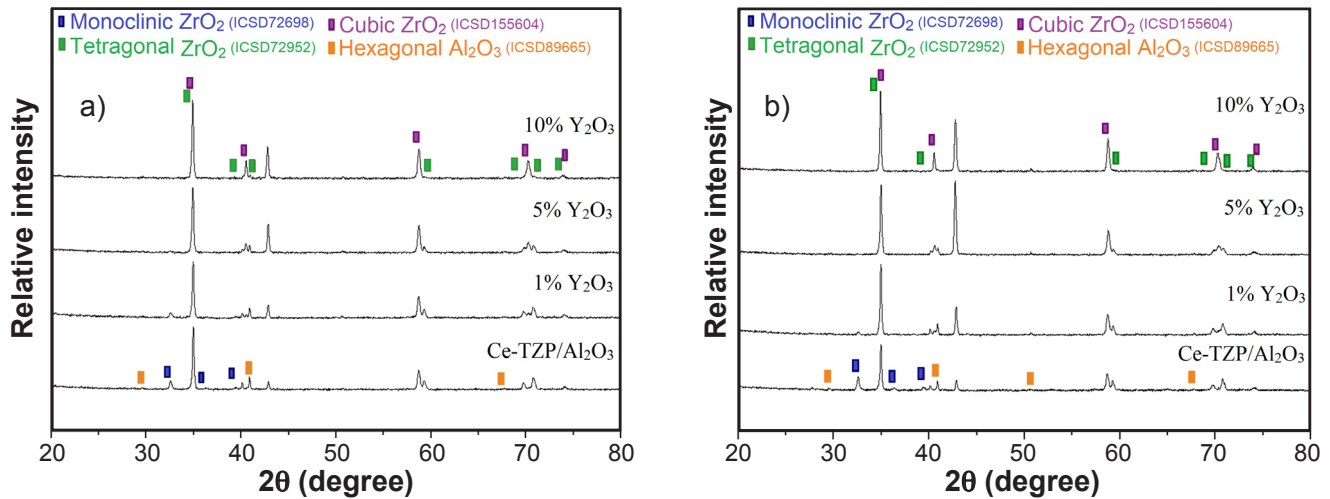


Figure 4: XRD patterns of Ce-TZP/Al₂O₃/Y₂O₃ composites sintered at: a) 1500 °C; and b) 1600 °C.

Table III - Quantification of zirconia polymorphs present in sintered samples.

Composition (wt% Y ₂ O ₃)	1500 °C			1600 °C		
	t-ZrO ₂ (%)	c-ZrO ₂ (%)	m-ZrO ₂ (%)	t-ZrO ₂ (%)	c-ZrO ₂ (%)	m-ZrO ₂ (%)
0%	83.2	6.4	10.4	64.8	6.9	28.3
1%	72.6	18.1	9.3	68.2	28.3	3.5
5%	47.9	52.1	0	37.4	62.6	-
10%	7.9	92.1	0	1.2	98.8	-

equipment at $2\theta=42.7^\circ$ was also identified. This pattern was maintained regardless of the sintering temperature. In order to promote a quantitative analysis, the diffractograms were analyzed using the Rietveld method. Table III shows the refinement results for the zirconia polymorphs found in the sintered composites. The formation of the t-ZrO₂ phase found in all composites, after sintering, came from the reaction that occurred between m-ZrO₂ and CeO₂ present in the commercial powder. In the samples containing 1 wt% Y₂O₃, a high amount of tetragonal phase (t-ZrO₂) was observed, which decreased as the sintering temperature increased. On the other hand, the samples doped with 5 and 10 wt% Y₂O₃ showed a different behavior, where the content of phase rich in Y₂O₃ (c-ZrO₂) increased as a function of the percentage of Y₂O₃. According to the literature [20], this occurred because there was a predisposition of the m-ZrO₂-Y₂O₃ system to form c-ZrO₂ at low temperatures. As the starting powder was basically composed of undoped ZrO₂ powder (Table II), it was expected that it would be more susceptible to the formation of c-ZrO₂ during the sintering process, due to the supply of Y₂O₃ in these powder mixtures. In the phase diagram of the ZrO₂-CeO₂ proposed by Li et al. [20], it is noticeable that the use of Y₂O₃ and CeO₂ tends to decrease the temperature according to the quantity used. However, Y₂O₃ is more effective; in this way, it is easier to form c-ZrO₂.

Fig. 5 presents the Raman spectra of the composites sintered at 1500 °C-2 h and 1600 °C-2 h and Table IV shows the wavenumbers of the peaks based on approximations

of the values found in the literature [21-26]. The bands corresponding to cubic and tetragonal zirconia generally show absorption characteristics at similar positions in the Raman spectrum [21]. However, as the amount of Y₂O₃ increased in the zirconia structure, shifts of the bands around 600 and 300 cm⁻¹ to lower wavenumbers were observed. This phenomenon was reported by Borik et al. [25]. Therefore, these shifts can be used to verify and demonstrate the incorporation of Y₂O₃ into the zirconia system. As the amount of Y₂O₃ increased in the initial composition of the mixture, a band shift was observed, 638 for 624 cm⁻¹ in samples sintered at 1500 °C and 640 for 620 cm⁻¹ in those sintered at 1600 °C. There was also a flattening of the 460 cm⁻¹ band for samples doped with 10% Y₂O₃. According to Hemberger et al. [27], this happened because with greater amounts of Y₂O₃, there was an increase in the ZrO₂ lattice parameters, replacement of Zr⁴⁺ ions by Y³⁺ ions, and an increase in the ionic bond strength between Zr-O due to the amount of O²⁻ vacancies. Yashima et al. [28] observed that as there was variation in the amount of Y₂O₃, there was a change in the Raman spectra of cubic and tetragonal ZrO₂. These changes were found in the 645 and 470 cm⁻¹ bands, however, the 470 cm⁻¹ band disappeared with increasing Y₂O₃ as it was prominent only in the t-ZrO₂ phase.

Fig. 6 shows SEM micrographs of the sintered specimens. In a qualitative analysis of the micrographs, it was possible to observe in the samples of Ce-TZP/Al₂O₃ and doped with 1 wt% of Y₂O₃ a microstructure with mostly submicrometric characteristics, in addition to equiaxed grains of Al₂O₃

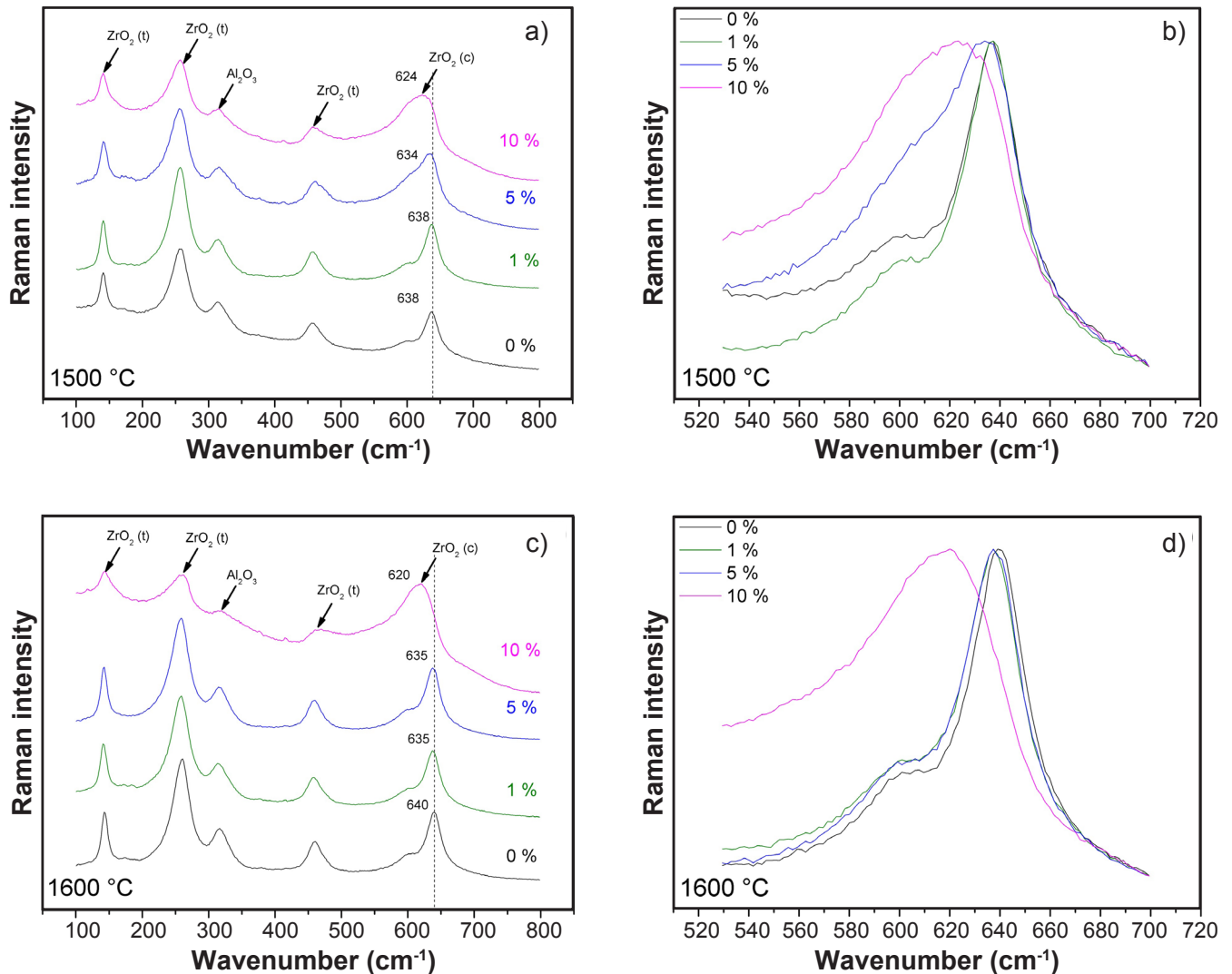


Figure 5: Raman spectra of the Ce-TZP/Al₂O₃ sintered at 1500 °C-2 h (a,b) and 1600 °C-2 h (c,d) with different Y₂O₃ contents.

Table IV - Theoretical wavenumbers (cm⁻¹) of Raman spectrum peaks of some bonds found in the prepared materials (values based on the literature [21-26]).

Zr-O (tetragonal)	Zr-O (cubic)	Al-O (α-alumina)
140	140	265
260	260	325
320	465	375
465	620	410
640	-	-

evenly distributed, preferably found in the triple junctions of ZrO₂ grains. However, in the samples doped with 5 and 10 wt% of Y₂O₃, a microstructure with a significantly larger grain fraction and a smaller average phase size could be seen. These characteristics were reported by other researchers [11, 29-31] who studied composite with a zirconia matrix. The grain size

analysis revealed that the alumina grains remained in the range of 0.1 to 0.8 μm in all composites, regardless of the amount of dopant and sintering temperature. In the sintering conditions analyzed, the zirconia grain size distribution remained between 0.1 to 3.3 μm, with an increase in the frequency of cubic (c-ZrO₂) grains as the temperature increased. On the other hand, the samples with 5 and 10 wt% of Y₂O₃ exhibited a grain size distribution with considerable growth, in the order of 0.1 to 4.9 μm, where there was a scattering of sizes in view of the different sintering temperatures.

Quantitatively, the literature indicates that the critical grain size of zirconia is close to 1~1.2 μm, which may be detrimental to the mechanical properties of the material [32-34]. Basu et al. [35] indicated that the increase in grain size may be related to the reduction of free energy in the grain boundaries, which consequently reduces the metastability of the t-ZrO₂ phase. According to the authors, this change in phase stability causes the grains to transform, consecutively inducing the transformation of neighboring grains in an

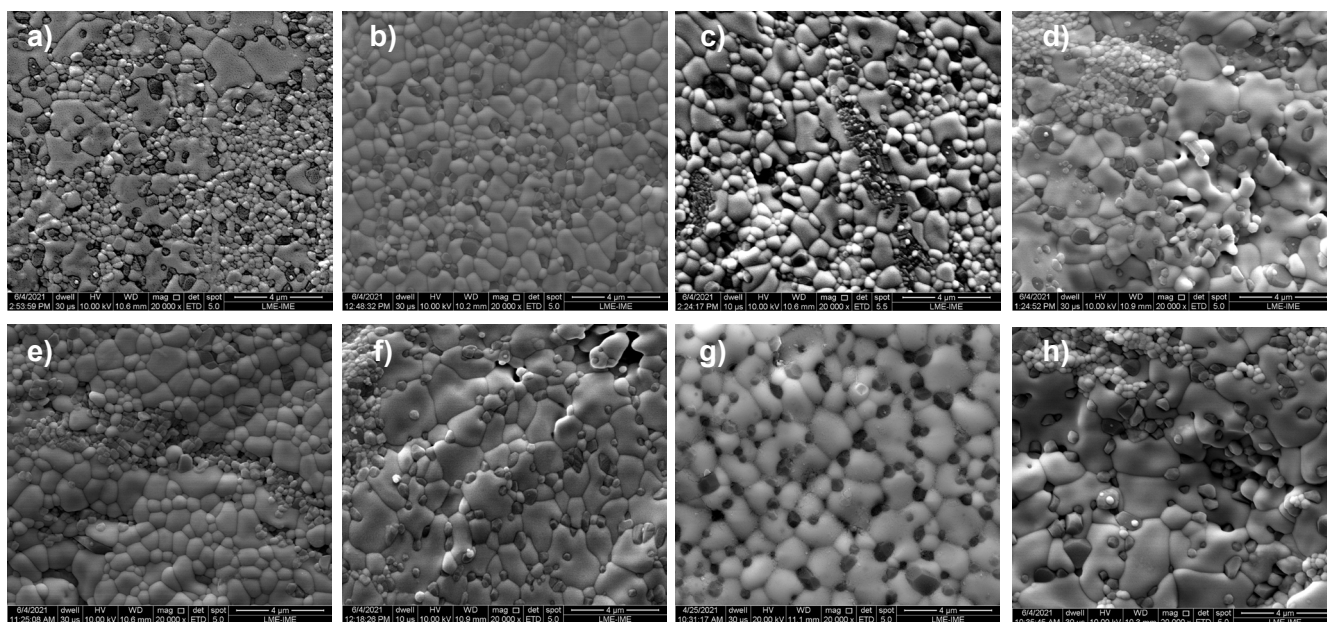


Figure 6: SEM micrographs of samples sintered at 1500 °C-2 h (a,c,e,g) or 1600 °C-2 h (b,d,f,h) containing 0 wt% (a,b), 1 wt% (c,d), 5 wt% (e,f), and 10 wt% (g,h) of Y_2O_3 .

autocatalytic way, where the transformation of the grain takes place by the stress field propagated by a nearby grain and not necessarily by the stress field of the crack propagation, which results in a more effective transformation zone. Taking into account that the grain growth increases as a function of the amount of Y_2O_3 [36, 37], it is acceptable that the specimens doped with 5 and 10 wt% of Y_2O_3 present a larger average grain size than those without additive and doped with 1% Y_2O_3 . Allemann et al. [37] and Matsui et al. [36] measured a grain size 30 times larger for c-ZrO₂ compared to t-ZrO₂. Therefore, this behavior can be related to the yttria diffusivity in the grain boundaries and the variation between the grain growth coefficients, tending to provide an increase in grains related to the phase rich in Y_2O_3 [36, 38, 39]. Alves et al. [30] observed that as the sintering temperature of the composites with higher contents of additive (Y_2O_3) increased, there was a significant increase in the average grain size from 0.62 μm (1475 °C) to 2.32 μm (1600 °C). Allemann et al. [37] studied

the growth of c-ZrO₂ phase grains according to the Y_2O_3 content of the initial powder, where they obtained both cubic and tetragonal phases with grain sizes in the order of 0.5 to 4.0 μm .

Table V presents the Vickers hardness and fracture toughness results for different composites sintered at 1500 or 1600 °C. The average values of Vickers hardness for composites sintered at 1500 and 1600 °C, respectively, were 11.9±0.3 and 12.0±0.2 GPa (Ce-TZP/ Al_2O_3), 12.3±0.3 and 12.1±0.2 GPa (1 wt% Y_2O_3), 11.3±0.6 and 11.5±0.6 GPa (5 wt% Y_2O_3), and 11.0±1.0 and 10.2±0.8 GPa (10 wt% Y_2O_3). There was no statistical difference between the hardness results obtained for materials sintered at different temperatures. Regarding the fracture toughness results, the values obtained at both sintering temperatures investigated were K_{IC} = 9.3±0.4 and 11.9 ± 0.3 $\text{MPa}\cdot\text{m}^{1/2}$ (Ce-TZP/ Al_2O_3), 10.5±0.6 and 9.1± 0.8 $\text{MPa}\cdot\text{m}^{1/2}$ (1 wt% Y_2O_3), 8.0±0.8 and 7.8±1.4 $\text{MPa}\cdot\text{m}^{1/2}$ (5 wt% Y_2O_3), and 5.8±0.9

Table V - Properties of the ceramic composites doped with Y_2O_3 .

Sample	Sintering temperature	Relative density (%)	Vickers hardness HV _{98N} (GPa)	Fracture toughness, $K_{IC,98N}$ ($\text{MPa}\cdot\text{m}^{1/2}$)
Ce-TZP/ Al_2O_3	1500 °C	92.7±2.1	11.9±0,3	9.3±0.4
Ce-TZP/ Al_2O_3 /1 wt% Y_2O_3		93.8±2.4	12.3±0.3	10.5±0.6
Ce-TZP/ Al_2O_3 /5 wt% Y_2O_3		92.4±3.4	11.3±0.6	8.0±0.8
Ce-TZP/ Al_2O_3 /10 wt% Y_2O_3		95.7±2.5	11.0±1.0	5.8±0.9
Ce-TZP/ Al_2O_3	1600 °C	94.5±0.4	12.0±0.2	11.9±0.3
Ce-TZP/ Al_2O_3 /1 wt% Y_2O_3		96.1±1.7	12.1±0.2	9.1±0.8
Ce-TZP/ Al_2O_3 /5 wt% Y_2O_3		95.3±3.0	11.5±0.6	7.8±1.4
Ce-TZP/ Al_2O_3 /10 wt% Y_2O_3		96.3±4.1	10.2±0.8	5.6±0.7

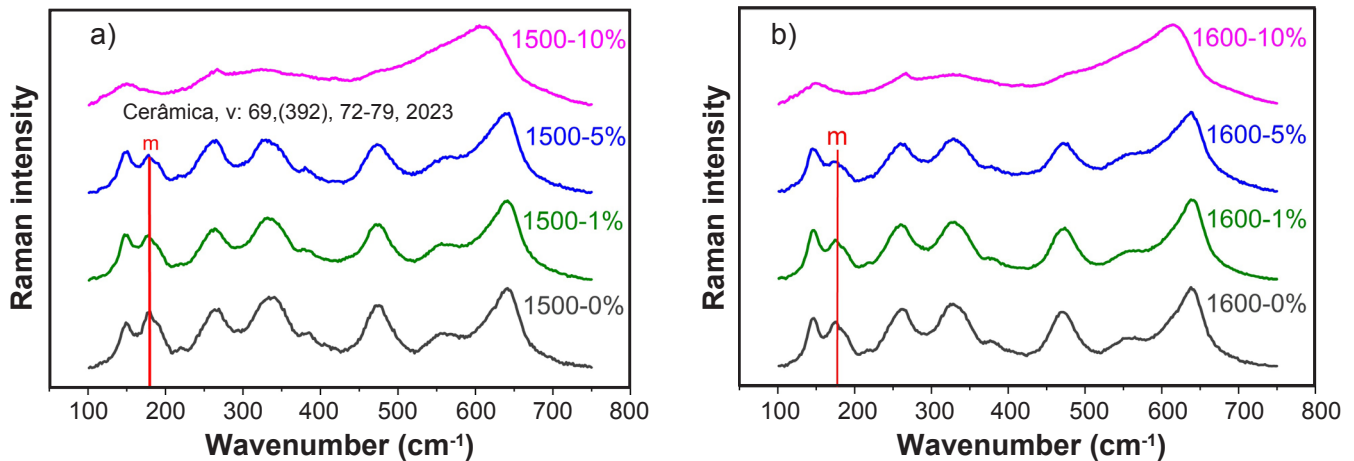


Figure 7: Raman spectra of the indentation regions in samples sintered at 1500 °C (a) and 1600 °C (b).

and $5.6 \pm 0.9 \text{ MPa}\cdot\text{m}^{1/2}$ (10 wt% Y₂O₃). The data found for the composites studied were close to those found by Cutler et al. [40] ($11.5 \pm 0.9 \text{ MPa}\cdot\text{m}^{1/2}$), Nawa et al. [11] ($8.5 \pm 0.2 / 11.0 \pm 0.3 \text{ MPa}\cdot\text{m}^{1/2}$), and Maleki et al. [41] ($7.83 \pm 0.13 / 11.0 \pm 0.2 \text{ MPa}\cdot\text{m}^{1/2}$), where Ce-TZP composites containing 15% to 30% Al₂O₃ were studied. As observed in the X-ray diffraction analyses, the use of Y₂O₃ induced the formation of c-ZrO₂ in addition to the formation of the t-ZrO₂ phase by stabilization with CeO₂. This microstructural configuration combined with densification allowed obtaining high values of fracture toughness. Considering the microstructure of the composites, it was possible to observe that as the amount of dopant (Y₂O₃) increased, there was a gradual decrease in hardness and fracture toughness. Tetragonal zirconia presents a peculiar toughening mechanism while the cubic phase does not. This mechanism is known as t→m phase transformation toughening, and when the grains expand, they create compression zones with a 3% to 5% increase in volume around the crack, making it difficult to propagate, in addition, the volumetric expansion forms microcracks around the grains dissipating the energy of the initial crack [42, 43].

This mechanism becomes more relevant when CeO₂ is used as opposed to Y₂O₃, since the shielding zone at the crack tip is larger, preventing the propagation of the same, helping the material to obtain a locking at the crack tip and consequently a high toughness to the crack fracture [42, 44-46]. In addition to the toughening mechanism by t→m phase transformation, another mechanism that must be considered is the deflection of cracks due to the existence of Al₂O₃ grains in the triple junctions of the zirconia grains [47], as it was possible to observe in the images of scanning electron microscopy, which act as a secondary mechanism of material toughening since the crack travels along the grain boundaries. Analysing Fig. 7, referring to the Raman spectra measured in the center of the indentations, it is possible to observe the martensitic transformation, revealed by the appearance of monoclinic (m-ZrO₂) phase bands that reveal the phase transformation, when comparing the Raman results presented in Fig. 5.

CONCLUSIONS

The addition of different contents of Y₂O₃ in ZrO₂-Al₂O₃-CeO₂ commercially available ceramic powder allowed to increase the fraction of cubic-ZrO₂ in the Ce-TZP-Al₂O₃ composites sintered at 1500 and 1600 °C. As expected, there was no significant reduction in the relative density and, consequently, in Vickers hardness of the composites. However, fracture toughness underwent progressive reduction due to the formation of cubic grains to the detriment of toughening ZrO₂-tetragonal grains. Considering the possible control of the cubic ZrO₂ phase content together with tetragonal grains present in the composite by the addition of Y₂O₃, future electronic applications can be prospected, requiring evaluations on the effects of alumina on the electrical properties of these composites, given the benefits of the mechanical strength of these composites.

ACKNOWLEDGMENTS

Dr. Eduardo de Sousa Lima would like to thank the National Council for Scientific and Technological Development - CNPq (project n° 312161/2020-4) for the financial support received. Dr. Claudinei Santos would like to thank FAPERJ (grant n° E-26/202.997/2017) and the National Council for Scientific and Technological Development - CNPq (project n° 311119/2017-4) for the financial support received.

REFERENCES

- [1] W.D. Kingery, H.K. Bowen, D.R. Uhlmann, *Introduction to ceramics*, Wiley (1976) 1056.
- [2] M.W. Barsoum, *Fundamentals of ceramics*, 2nd ed., Taylor Francis (2003) 27.
- [3] R. Stevens, *Zirconia and zirconia ceramics*, 2nd ed., Magnesium Elektron, Twickenham (1986) 56.
- [4] K. Tsukuma, M. Shimada, *J. Mater. Sci.* **20**, 4 (1985) 1178.

- [5] J. Chevalier, L. Gremillard, A.V. Virkar, D.R. Clarke, J. Am. Ceram. Soc. **92**, 9 (2009) 1901.
- [6] J.D. Lin, J.G. Duh, Mater. Chem. Phys. **78**, 1 (2003) 253.
- [7] M. Inokoshi, F. Zhang, J.D. Munck, S. Minakuchi, I. Naert, J. Vleugels, B.V. Meerbeek, K. Vanmeensel, Dent. Mater. **30**, 6 (2014) 669.
- [8] J. Chevalier, Biomaterials **27**, 4 (2006) 535.
- [9] A. Ueno, M. Nawa, K. Omori, N. Kurizoe, J. Eur. Ceram. Soc. **37**, 2 (2017) 679.
- [10] M. Taya, S. Hayashi, A.S. Kobayashi, H.S. Yoon, J. Am. Ceram. Soc. **73**, 5 (1990) 1382.
- [11] M. Nawa, S. Nakamoto, T. Sekino, K. Niihara, Ceram. Int. **24**, 7 (1998) 497.
- [12] F. Marro, A. Mestra, M. Anglada, J. Eur. Ceram. Soc. **31**, 13 (2011) 2189.
- [13] S. Tekeli, A. Kayış, M. Gürü, J. Solid State Electrochem. **12** (2008) 791.
- [14] ASTM C1327-15, "Standard test method for Vickers indentation hardness of advanced ceramics", ASTM Int., West Conshohocken (2015).
- [15] K. Niihara, J. Mater. Sci. Lett. **2** (1983) 221.
- [16] D.R. Clarke, F. Adar, J. Am. Ceram. Soc. **65**, 6 (1982) 284.
- [17] F. Lange, J. Eur. Ceram. Soc. **28**, 7 (2008) 1509.
- [18] S. Naga, A. Hassan, H. El-Maghraby, M. Awaad, Ceram. Int. **45**, 2 (2019) 1634.
- [19] S. Naga, E. Abdelbary, M. Awaad, Y. El-Shaer, H. Abd-Elwahab, Ceram. Int. **39**, 2 (2013) 1835.
- [20] L. Li, O.V.D. Biest, P. Wang, J. Vleugels, W. Chen, S. Huang, J. Eur. Ceram. Soc. **21**, 16 (2001) 2903.
- [21] C. Wulfman, M. Sadoun, M.L. De La Chapelle, IRBM **31**, 5-6 (2010) 257.
- [22] C.A. Goulart, M.M. de Toledo Piza, T.M.B. Campos, E.A. Bonfante, P.N. Lisboa Filho, Ceram. Int. **49**, 13 (2023) 22076.
- [23] T.M.B. Campos, R.M. de Melo Marinho, A.D.O.P. Ribeiro, T.L. do Amaral Montanheiro, A.C. da Silva, G.P. Thim, J. Mech. Behav. Biomed. Mater. **113** (2021) 104093.
- [24] F. Gyakwaa, T. Alatarvas, Q. Shu, M. Aula, T. Fabritius, Metals **11**, 10 (2021) 1549.
- [25] M.A. Borik, S.I. Bredikhin, V.T. Bublik, A.V. Kulebyakin, I.E. Kuritsyna, E.E. Lomonova, F.O. Milovich, V.A. Myzina, V.V. Osiko, P.A. Ryabochkina, N. Yu. Tabachkova, T.V. Volkova, Mater. Lett. **205** (2017) 186.
- [26] P.H. Pessoa, L.K.S. Assis, E.L.T. França, A.S. Carvalho, D.M. Oliveira, E. Padrón-Hernández, J. Sol-Gel Sci. Technol. **108**, 1 (2023) 1.
- [27] Y. Hemberger, N. Wichtner, C. Berthold, K.G. Nickel, Appl. Ceram. Technol. **13**, 1 (2015) 116.
- [28] M. Yashima, K. Ohtake, M. Kakihana, H. Arashi, M. Yoshimura, J. Phys. Chem. Solids **57**, 1 (1996) 17.
- [29] M.F.R.P. Alves, L.G. Abreu, G.G. Klippel, C. Santos, K. Strecker, Ceram. Int. **47**, 1 (2021) 301.
- [30] M.F.R.P. Alves, S. Ribeiro, P.A. Suzuki, K. Strecker, C. Santos, Mater. Res. **24**, 2 (2021) e20200402.
- [31] S. Naga, A. Hassan, H. El-Maghraby, M. Awaad, Ceram. Int. **45**, 2 (2019) 1634.
- [32] J. Wang, R. Stevens, J. Mater. Sci. **24**, 10 (1989) 3421.
- [33] R. Shahmiri, O.C. Standard, J.N. Hart, C.C. Sorrell, J. Prosthet. Dent. **119**, 1 (2018) 36.
- [34] Y. Zhang, Dent. Mater. **30**, 10 (2014) 1195.
- [35] B. Basu, J. Vleugels, O.V.D. Biest, Mater. Sci. Eng. A **366**, 2 (2004) 338.
- [36] K. Matsui, T. Yamakawa, M. Uehara, N. Enomoto, J. Hojo, J. Am. Ceram. Soc. **91**, 6 (2008) 1888.
- [37] J. Allemann, B. Michel, H.B. Märki, L. Gauckler, E. Moser, J. Eur. Ceram. Soc. **15**, 10 (1995) 951.
- [38] K. Matsui, H. Yoshida, Y. Ikuhara, J. Eur. Ceram. Soc. **30**, 7 (2010) 1679.
- [39] K. Matsui, H. Yoshida, Y. Ikuhara, Int. Mater. Rev. **63**, 6 (2017) 375.
- [40] R.A. Cutler, R.J. Mayhew, K.M. Prettyman, A.V. Virkar, J. Am. Ceram. Soc. **74**, 1 (1991) 179.
- [41] M. Maleki, S.M. Sheikh-Al-Eslamian, E. Hasani, A. Ghasemi, J. Alloys Compd. **776** (2019) 166.
- [42] B. Basu, Int. Mater. Rev. **50**, 4 (2005) 239.
- [43] G. Gregori, W. Burger, V. Sergo, Mater. Sci. Eng. A **271**, 1-2 (1999) 401.
- [44] R.C. Garvie, M.F. Goss, J. Mater. Sci. **21**, 4 (1986) 1253.
- [45] L. Rose, M. Swain, Acta Metall. **36**, 4 (1988) 955.
- [46] G. Rauchs, T. Fett, D. Munz, R. Oberacker, J. Eur. Ceram. Soc. **21**, 12 (2001) 2229.
- [47] M. Hablitzel, D. Garcia, D. Hotza, Matéria **16**, 3 (2011) 788.

(Rec. 11/07/2023, Rev. 29/09/2023, Ac. 20/10/2023)

